JPE 17-1-21

https://doi.org/10.6113/JPE.2017.17.1.212
ISSN(Print): 1598-2092 / ISSN(Online): 2093-4718

Control and Analysis of Vienna Rectifier Used as the Generator-Side Converter of PMSG-based Wind Power Generation Systems

Hongyan Zhao†, Trillion Q. Zheng*, Yan Li*, Jifei Du*, and Pu Shi*

†,*School of Electrical Engineering, Beijing Jiaotong University, Beijing, China

Abstract

Permanent-Magnet Synchronous Generators (PMSGs) are used widely in Wind Power Generation Systems (WPGSs), and the Vienna rectifier was recently proposed to be used as the generator-side converter to rectify the AC output voltage in PMSG-based WPGS. Compared to conventional six-switch two-level PWM (2L-PWM) converters, the Vienna rectifier has several advantages, such as higher efficiency, improved total harmonic distortion, etc. The motivation behind this paper is to verify the performance of direct-driven PMSG wind turbine system based-Vienna rectifier by using a simulated direct-driven PMSG WPGS. In addition, for the purpose of reducing the reactive power loss of PMSGs, this paper proposes an induced voltage sensing scheme which can make the stator current maintain accurate synchronization with the induced voltage. Meanwhile, considering the Neutral-Point Voltage (NPV) variation in the DC-side of the Vienna rectifier, a NPV balancing control strategy is added to the control system. In addition, both the effectiveness of the proposed method and the performance of the direct-driven PMSG based-Vienna rectifier are verified by simulation and experimental results.

Key words: Induced voltage, Neutral-Point Voltage (NPV), Permanent-Magnet Synchronous Generator (PMSG), Vienna rectifier

I. INTRODUCTION

It is well known that the use of renewable power systems is becoming more and more important in terms of reducing fossil energy depletion [1]-[3], and the Wind Power Generation Systems (WPGSs) are perhaps the most widely used renewable power system. It is due in large part to its cost effectiveness and high reliability. In particular, the application of direct-driven Permanent-Magnet Synchronous Generation (PMSG) WPGS is a trend in the development of WPGS applications, especially in offshore and home scale WPGSs [4]-[9]. As a result, in order to decouple the speed of a PMSG from a grid, especially when all of the energy should go through the grid interface system [10], [11], the demand for power electronic devices with a higher rating at a lower cost has risen, as shown in Fig. 1.

Compared to conventional doubly fed induction generators (DFIGs), PMSGs have some inherent benefits and drawbacks when used in the WPGS, as listed in the followings [11].

Benefit 1: A multistage gearbox is obligatory for DFIG-based systems. However, they are not needed in PMSG-based systems.

Benefit 2: The design of the low voltage ride-through (LVRT) capability in DFIG-based systems is more intricate than that in PMSG-based systems [12].

Benefit 3: Since the rotor windings are connected to a power converter, a slip-ring is used in DFIG-based WPGSs.

Drawback 1: PMSGs are more expensive than DFIGs.

Drawback 2: Only a partial-scale power converter is needed in DFIG-based systems, while a full-scale power converter is necessary in PMSG-based systems [11].

It is widely known that the common topologies widely used as the generator-side converters in both PMSG-based and DFIG-based WPGSs are three-phase uncontrolled diode-bridge rectifier (U-DBR) [13] and six-switch two level PWM (2L-PWM) converters [14], which are both full-scale power converters.

When a three-phase U-DBR is applied as the generator-side converter, a DC/DC converter [15] or a

Manuscript received Apr. 8, 2016; accepted Sep. 20, 2016
Recommended for publication by Associate Editor Dong-Myung Lee.
†Corresponding Author: 13117367@bjtu.edu.cn
Tel: +86-010-51684911, Beijing Jiaotong University
*School of Electrical Engineering, Beijing Jiaotong University, China

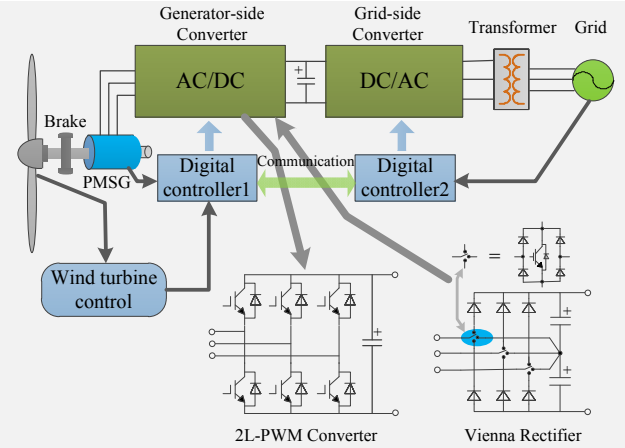

Fig. 1. Grid-connection with direct-driven PMSG-based WPGS.

Z-source inverter [16] is needed to satisfy the requirement of controlling the dc-bus voltage to adjust the speed of the PMSG. It is well known that the U-DBR has the benefits of high reliability and low cost. However, compared to 2L-PWM converters, the U-DBR has the following drawbacks which limit its application prospects: 1) the Power Factor (PF) is uncontrolled; 2) the Total Harmonic Distortion (THD) of the current is high; and 3) serious torque oscillations result in a lifetime reduction and an efficiency decrease. Therefore, due to the drawbacks of the U-DBR, a 2L-PWM converter is the prevailing choice [11]. Aside from the three-phase U-DBR, since the 2L-PWM converter has six power switches, for decreasing the system cost of direct-driven PMSG-based WPGS such as generator-side converters, some topologies which reduce the number of power switches have been investigated [17]-[22].

The Vienna rectifier is a three-level unidirectional rectifier proposed by professor Kolar, in 1997. Several advantages of Vienna rectifier, as listed in the following, make it a good choice to be used as the generator-side converter of PMSG-based WPGSs [23]: 1) it outputs two equal dc voltages—this provides a good choice to use a three-level NPC inverter as the grid-side converter [24]; 2) ti has a low manufacturing cost—using only three power switches, with half voltage stress compared to conventional 2L-PWM converters; 3) it possesses a high power quality—because of the three-level rectifier topology, the THD is inherently lower than 2L-PWM converters [11]; and 4) it has a high efficiency—as described in [21] and [22], Vienna rectifier has a higher efficiency compared to conventional 2L-PWM converters. Therefore, in some occasions, such as multi-MW PMSG-based WPGS and the need for a low THD and a higher efficiency, the Vienna rectifier is a good choice to be used as the generator-side converter. In conclusion, the topologies of both the 2L-PWM converter and the Vienna rectifier when used as generator-side converters are drawn out in Fig. 1, and a comparison between the two converters is given, as shown in Table I.

TABLE I
COMPARISON BETWEEN VIENNA RECTIFIER AND 2L-PWM CONVERTER

Specifications	2L-PWM converter	Vienna rectifier
3-level or not	no	yes
Number of power switches	6	3
THD	high	low
Efficiency	low	high
Power flow direction	bidirectional	unidirectional
Voltage stress of switch	V_{dc}	$V_{dc}/2$

In this paper, a simulated direct-driven PMSG-based WPGS which uses the Vienna rectifier as the generator-side converter is established. Moreover, for purpose of reducing the reactive power loss of a PMSG, an induced voltage sensing scheme is proposed, which can make the stator current maintain accurate synchronization with the induced voltage. Obviously, the proposed method eliminates the phase difference between the induced voltage and the stator current, which influences the stator winding inductance. The proposed induced voltage sensing scheme is implemented by detecting the position of the rotor and the phase angle of the induced voltage. As a result, a robust control with a well-regulated DC voltage and a good stator current quality is verified through simulation and experimental results.

II. PMSG MODEL AND VIENNA RECTIFIER OPERATION

A. Model of a PMSG

Generally speaking, before establishing the mathematical voltage model of a PMSG, the positive direction of the related physical variables should be defined. The positive direction of the three-phase current is the positive output direction of the three-phase induced voltage, and the positive direction of the three-phase flux is the positive direction of the three-phase stator winding axle. In addition, according to the Kirchhoff current law (KCL) and the Kirchhoff voltage law (KVL), the mathematical voltage equation of a PMSG in the three-phase stationary *a-b-c* reference frame can be obtained by:

$$\begin{bmatrix} v_a \\ v_b \\ v_c \end{bmatrix} = -\begin{bmatrix} R_s + p(L+\frac{1}{2}M) & 0 & 0 \\ 0 & R_s + p(L+\frac{1}{2}M) & 0 \\ 0 & 0 & R_s + p(L+\frac{1}{2}M) \end{bmatrix} \cdot \begin{bmatrix} i_a \\ i_b \\ i_c \end{bmatrix} + \begin{bmatrix} e_a \\ e_b \\ e_c \end{bmatrix} \quad (1)$$

where v_x (x=a,b,c) is the three-phase output voltage of the stator winding, i_x is the three-phase stator current, and e_x is the three-phase induced voltage. M is the mutual-inductance among the stator windings, L is the self-inductance of the

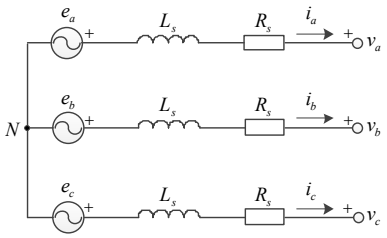

Fig. 2. Simplified equivalent physical model of PMSG in stationary *a-b-c* frame.

stator winding, and $L=M+l_r$, where l_r is the leakage inductance of the stator winding, and R_s is the equivalent resistance of the stator winding. w_e is the angular velocity of e_x, and θ_e is the rotor position angle described in the form of electricity, i.e., the phase angle of e_x, and p is the derivative.

As a result, with Equ. (1) and defining $L_s=L+M/2$, it is possible to obtain the simplified equivalent physical model of a PMSG in the stationary *a-b-c* frame, as shown in Fig. 2.

Furthermore, according to the law of electromagnetic induction, the induced voltage can be obtained as follows:

$$\begin{cases} e_a = p\psi_{fa} = -\omega_e\psi_f \sin(\theta_e + \varphi_e) \\ e_b = p\psi_{fb} = -\omega_e\psi_f \sin(\theta_e + \varphi_e - 2\pi/3) \\ e_c = p\psi_{fc} = -\omega_e\psi_f \sin(\theta_e + \varphi_e + 2\pi/3) \end{cases} \quad (2)$$

where ψ_{fx} is the three-phase rotor flux of the PMSG, and φ_e is the original phase angel of the induced voltage e_a.

B. Operation of the Vienna Rectifier

Considering the simplified equivalent model of PMSG, the topology of Vienna rectifier is redrawn in Fig. 3. In Fig. 3, S_x is the power switch. C_1 and C_2 are the filter capacitors in the DC side. i_p and i_n are the charge/discharge currents of C_1 and C_2, respectively. i_o is the neutral-point current of the DC side.

It is well known that each power switch in Vienna rectifier has two states, i.e., on and off (1 and 0). Therefore, there are a total of 8 (2^3=8) switching state combinations. It is apparent that, at any time, the switching state of the three power switches is one of 8 combinations. Meanwhile, the 8 switching state combinations are given in Table II .

III. Rotor Position Detection and Induced Voltage Sensing

A. Position Detection of the Rotor

PhotoElectric Encoder (PEE) is widely used on occasions where there is a need to detect the rotating speed. The PEE is directly connected to the axle of the PMSG rotor and keeps rotating synchronously with the PMSG rotor. It is obvious that, with PEE, the space position variation of the PMSG rotor can finally be converted to a digital signal. As a consequence, the position and speed of the PMSG rotor can be obtained in DSP. In this paper, an incremental rotary encoder is adopted. This kind of encoder generates three square pulse wave signals, i.e., pulse-A, pulse-B and pulse-Z. Moreover, it should be pointed out that pulse-A and pulse-B

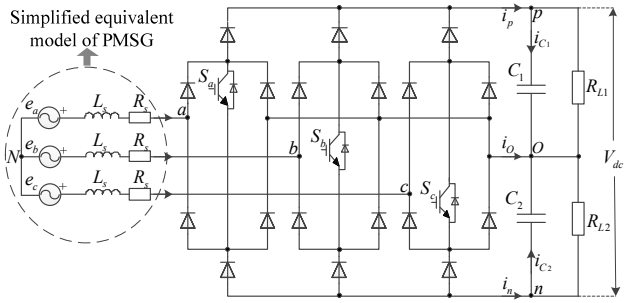

Fig. 3. Schematic diagram of Vienna rectifier.

TABLE II
Combinations of the Switching States

Switches	Switching states							
S_a	0	0	0	0	1	1	1	1
S_b	0	0	1	1	0	0	1	1
S_c	0	1	0	1	0	1	0	1

are two orthogonal square waves. Therefore, it is possible to obtain the rotating direction of the PMSG rotor by the relative positions of pulse-A and pulse-B. Furthermore, it is possible to obtain the rotating speed of the PMSG rotor by calculating the number of pulse-A and pulse-B. In addition, theoretically there is only one pulse-Z in every machine cycle of the PMSG rotor, and the position of the pulse-Z is fixed to the position of the rotor. Thus, with pulse-Z, the position of the PMSG rotor can finally be obtained.

It is widely known that the induced voltage of a PMSG should be sensed by some specific methods. This is due to the fact that it cannot be measured directly by a voltage sensor. To obtain the induced voltage, as known from Equ. (2), the original phase angel φ_e of e_a should be obtained first. However, φ_e is decided by the original position of the PMSG rotor. Therefore, the rotor's original position detection is the primary task. Because of this, a rotor's original position detection method is proposed in this paper.

Generally speaking, the stator winding output voltage v_x can be measured by a voltage sensor, and the induced voltage e_x is equal to v_x when the PMSG is under the condition of no-load, i.e., $e_x=v_x$. Therefore, under the condition of no-load, the original position of the PMSG rotor (the position of pulse-Z) and the original phase angel φ_e of e_a can be obtained by v_x and pulse-A, pulse-B and pulse-Z.

Assuming that the grating number of a PEE is N, then it can generate N pulse-A and N pulse-B in one machine cycle T_Z of the PMSG rotor. As a result, there is a total of 2N pulses and 4N pulse edge signals (including the positive edge and the negative edge) which are represented by a digital counter n in one machine cycle. It is obvious that the max value n_{max} of n is 4N, i.e., n_{max}=4N. Furthermore, if the pole-pair of the PMSG is p_0, then the induced voltage period T_e is $1/p_0$ of T_Z, i.e., $T_e=T_Z/p_0$. Correspondingly, the induced voltage counter n_e is n/p_0 in every induced voltage period, i.e., $n_e=n/p_0$. In addition, the max value n_{emax} of n_e is n_{max}/p_0, i.e.,

n_{emax}= n_{max}/p_0. Theoretically, when the PEE is connected to the PMSG rotor and rotates synchronously with the PMSG rotor, the position of pulse-Z is fixed to the position of the rotor. Therefore, pulse-Z will be generated in a certain fixed value n_Z of n in every machine cycle. Finally, n_Z can be regarded as the position of pulse-Z.

When the system starts to run and the PMSG starts to rotate without a load, an induced voltage is generated. Then the position detection process of pulse-Z can be started. First, select one negative zero crossing point (N-ZCP) of v_a, i.e., the value of v_a from positive to negative, and regard this N-ZCP as the start point of the position detection process. Second, at the moment of N-ZCP of v_a, counter n starts counting from 0 and, counter n_e starts counting from 0 to n_{emax} periodically. In addition, the expected phase angle θ_e of the induced voltage e_a increases periodically from 0 to 2π with a step of $2\pi/n_{emax}$. Therefore, n_e and θ_e have the same period, i.e., both n_e and θ_e are reset to 0 when n_e=n_{emax}. Moreover, in the course of n counts, if pulse-Z arises and n belongs to the range of 0 to n_{max} at the same time, record the values n_i of n, n_{ei} of n_e and θ_{ei} of θ_e at this moment. In addition, let the variable φ_{ei}=θ_{ei}, then n_i can be regarded as the position of pulse-Z, and φ_{ei} can be regarded as the original phase angle of the induced voltage e_a. However, if pulse-Z arises and n exceed the range of 0 to n_{max}, it means that one pulse-Z is lost. Then reset all of the counters n, n_e and θ_e to 0, and restart the position detection process of pulse-Z from another N-ZCP of induced voltage e_a. Finally, repeat the detection process k (i=1,2…k) times and obtain the average values n_Z of n_i and φ_e of φ_{ei} among the k times, respectively, i.e.:

$$n_Z = \frac{1}{k}\sum_{i=1}^{k} n_i \text{ and } \varphi_e = \frac{1}{k}\sum_{i=1}^{k} \varphi_{ei} \tag{3}$$

As a result, n_Z and φ_e are regarded as the final position of pulse-Z and the original phase angle of the induced voltage e_x, respectively.

Referring to the specifications of the PEE and PMSG applied in this paper, it can know that the grating number N of the PEE is 2000, and the pole-pair p_0 of the PMSG is 8. Therefore, n_{max}=4N=8000 and n_{emax}=n_{max}/8=1000 can be directly obtained. In conclusion, the position detection principle and process of pulse-Z are shown in Fig. 4 and Fig. 5, respectively.

B. Sensing of the Induced Voltage

It is well know that if the gratings of the PEE are N, the rotating speed distinguishability is 1/N; and if the counter n is increased by m in the period of ΔT, the mechanical angle variation $\Delta\theta_r$ of the rotor position is $2\pi m$/4N, i.e., $\Delta\theta_r$=$2\pi m$/4N. Then the mechanical angular velocity of the rotor can be obtained as:

$$\omega_r = \frac{\Delta\theta_r}{\Delta T} = \frac{2\pi m}{4N\Delta T}. \tag{4}$$

In addition, according to the pole-pair p_0 of the PMSG, the angular velocity of the induced voltage can be calculated by:

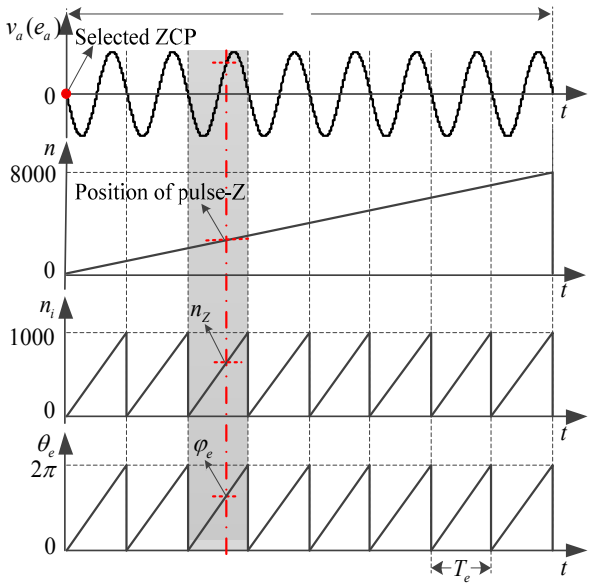

Fig. 4. Position detection principle of pulse-Z.

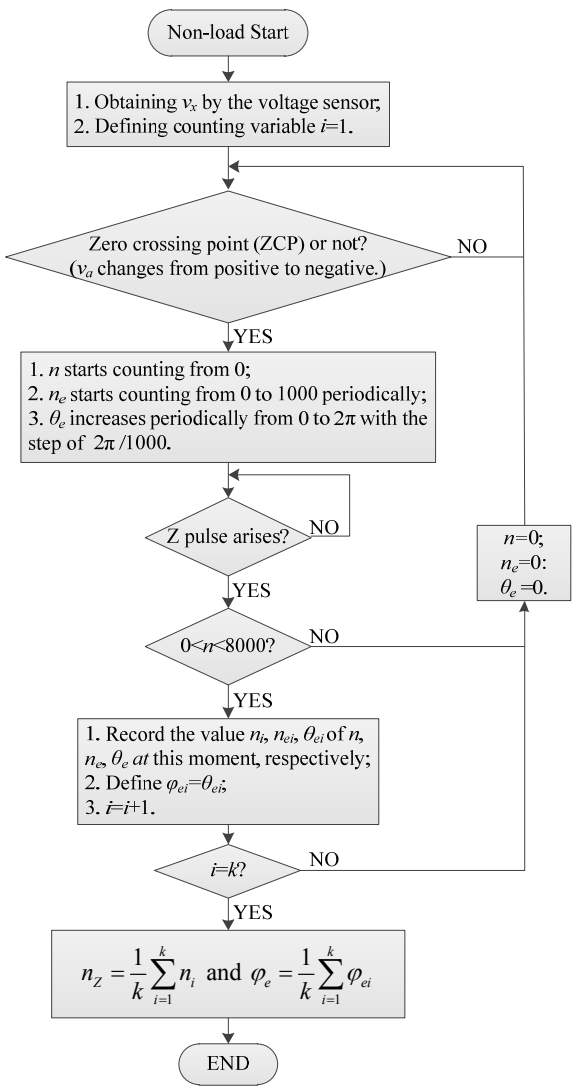

Fig. 5. Position detection process of pulse-Z.

$$\omega_e = p_0 w_r = \frac{2\pi m p_0}{4N\Delta T}. \quad (5)$$

Therefore, the phase angle of e_a can be obtained as:

$$\theta_e = w_e t + \varphi_e \quad (6)$$

In particular, it should be noted that due to the mechanical error between the PMSG axle and the PEE center, m has an inevitably error. Therefore, to eliminate the accumulative error of θ_e, θ_e is reset to φ_e every time pulse-Z arises.

Finally, the three-phase induced voltage can be obtained by submitting the w_e and φ_e into Equ. (2). Take e_a as an example below.

$$\begin{aligned} e_a(t) &= \frac{d\psi_r}{dt} = \frac{d\psi_{r\max}\cos(\omega_e t + \varphi_e)}{dt} \\ &= -\omega_e \psi_{r\max}\sin(\omega_e t + \varphi_e) \end{aligned} \quad (7)$$

where ψ_{rmax} is the magnetic flux linkage of rotor.

Furthermore, it can be seen in Equ. (7) that the amplitude and frequency of the induced voltage of the PMSG change with the rotor speed.

IV. Control Strategy

The commonly used control strategy of PMSG-based WPGSs is shown in the control diagram in Fig. 6. From Fig. 6 it can be seen that the main purpose of the generator-side converter is to control a PMSG to realize the maximum power point tracking (MPPT) and to keep the system working at the state of the unit power factor (PF=1), while the grid-side converter is mainly used to control the DC link voltage and to adjust the grid-connected active power and reactive power.

However, this paper focuses on the generator-side when the Vienna rectifier is used as the generator-side converter. Therefore, for the purpose of keeping the DC link voltage at the steady state, the out-loop MPPT controller of the generator-side is replaced by a DC link voltage controller, i.e., PART A is replaced by PART B in Fig. 6.

This paper adopts a double-loop control strategy in the synchronous rotating d-q reference frame, i.e., the DC link voltage out-loop control and the current inner-loop control. A mathematical model of the Vienna rectifier in the synchronous rotating d-q reference frame can be expressed in the form of:

$$\begin{cases} L_s\, di_d/dt = -R_s i_d + \omega_e L_s i_q - v_d + e_d \\ L_s\, di_q/dt = -R_s i_q + \omega_e L_s i_d - v_q + e_q \end{cases} \quad (8)$$

All the three-level converters have a problem of NPV variation which is determined by the topology nature of the three-level converters. The NPV variation, i.e., $V_{C1} \neq V_{C2}$, is mainly caused by the following conditions: the loads are unbalanced, the parameters of C_1 and C_2 are unequal, the parameters of the three power switches are inconsistent with each other and so on. In addition, the fluctuations of the three-phase input voltage can also result in NPV variations. Therefore, NPV balancing control in three-level converters is a key problem. In the Vienna rectifier, the voltages of the capacitors C_1 and C_2 can be derived as:

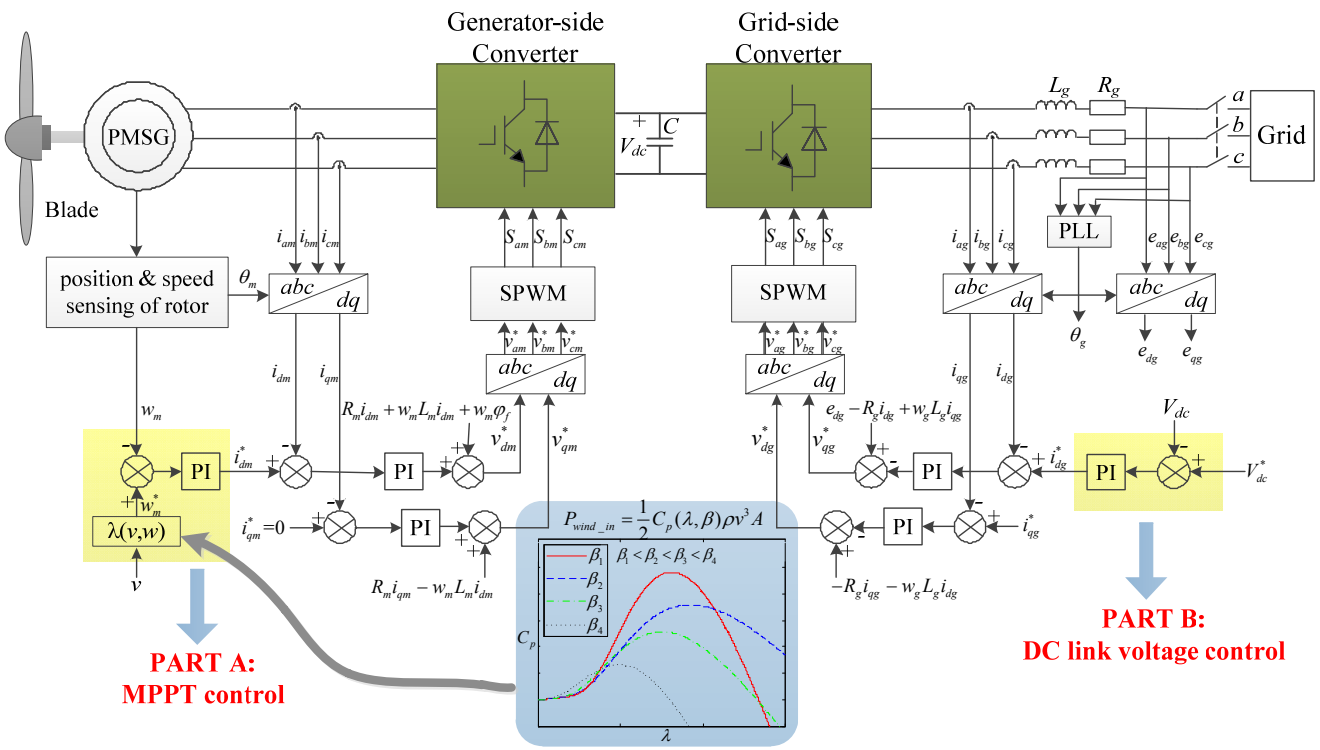

Fig. 6. Common used control strategy of PMSG-based WPGS.

$$\begin{cases} V_{C1} = \dfrac{1}{C_1}\int_{t_1}^{t_2} i_{C1}dt \\ V_{C2} = -\dfrac{1}{C_2}\int_{t_1}^{t_2} i_{C2}dt \end{cases} \quad (9)$$

Moreover, when C_1 and C_2 satisfy that C_1=C_2=C, the NPV can be obtained as:

$$\Delta V_C = V_{C1} - V_{C2} = \frac{1}{C}\int_{t_1}^{t_2} i_{C1} + i_{C2}dt = -\frac{1}{C}\int_{t_1}^{t_2} i_O dt. \quad (10)$$

According to Equ. (10), it is apparent that the NPV is decided by the flow of the current i_O. furthermore, the current i_O can be controlled by modifying the modulation waves. The modifying strategy is to add an offset v_{sh} which is obtained by applying a PI controller to the modulation waves. Finally, the control strategy of the NPV is shown in Fig. 7.

However, there is a fact should be noted that the stator current quality of the PMSG is inevitably affected by the modification of the modulation waves, and this is the main shortcoming of the NPV balancing control strategy with Vienna rectifier.

The entire control structure, adopted in this paper, of the generator-side is given in Fig. 8.

V. Simulation and Experiment Verification

A. Simulation Verification

It can be seen in Equ. (7) that the amplitude and frequency of the induced voltage changes with the rotating speed. Therefore, for simulating the conditions of the rotating speed change in the direct-driven PMSG-based WPGS, the amplitude and frequency of the three-phase voltage change with respect to time in the simulation.

Fig. 9 gives simulation result of the generator-side. Before 0.1 s, the Vienna rectifier works in the un-controlled state to charge the capacitors C1 and C_2. At 0.1 s, the system is switched to the double-loop control state. The amplitude and frequency of the given three-phase voltage are 187 V/30 Hz and the DC voltage reference value is 480 V dc. At 0.3 s, the three-phase voltage and the DC voltage reference changed to 249 V/40 Hz and 800 V dc, respectively. Then when the simulation runs at 0.5 s, the three-phase voltage is changed to 311 V/50 Hz, and the DC voltage reference value remains unchanged at 800 V dc. From the simulation results, it can be seen that the performance of the double-loop control strategy is good and robust when the three-phase voltage changes with time.

Fig. 10 and Fig. 11 show comparison results in the conditions of before and after adding the NPV voltage control strategy when the loads are unbalanced. Fig. 10 (a) correspond to the simulation of without the NPV control strategy. It can be clearly seen from Fig. 10 (a) that due to the unbalanced loads, the voltages of capacitors C_1 and C_2 are unequal. However, when the NPV control strategy is added to the control system, the two voltages of C_1 and C_2 can be kept

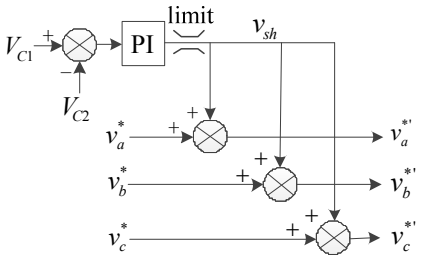

Fig. 7. Control strategy of NPV.

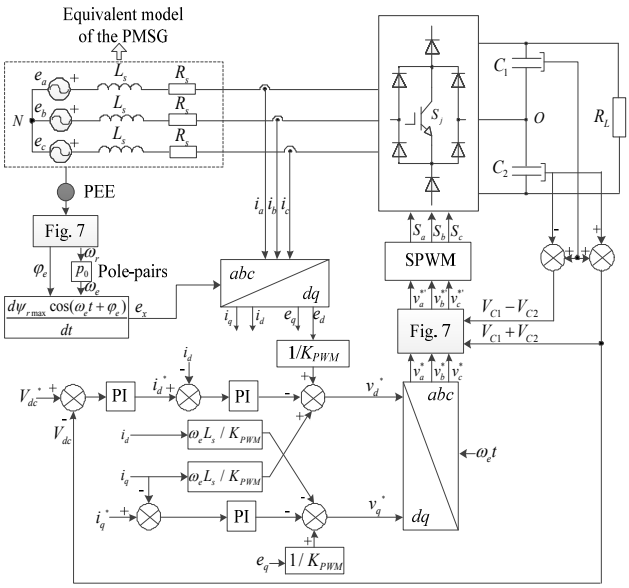

Fig. 8. The adopted control diagram of Vienna rectifier used as the generator-side converter.

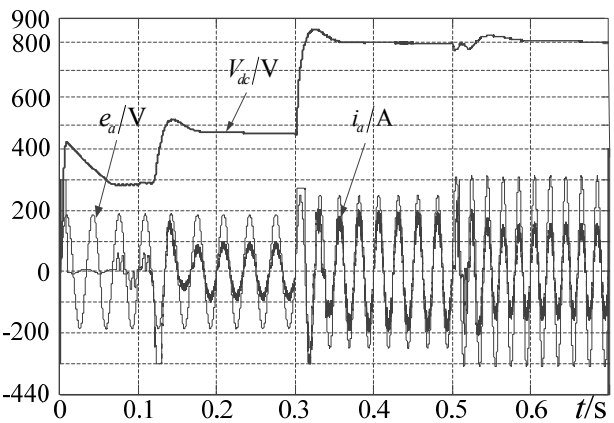

Fig. 9. Simulation results in the mode of simulated direct-driven PMSG-based WPGS.

balanced as shown in Fig. 10(b). In addition, NPV waveforms before and after adding the NPV control strategy are given in Fig. 11 (a) and (b), respectively. From Fig. 11 it can be seen that with the NPV control strategy, the NPV can be kept balanced when the loads are unbalanced. Both Fig. 10 and Fig. 11 verify the effectiveness of the adopted NPV control strategy.

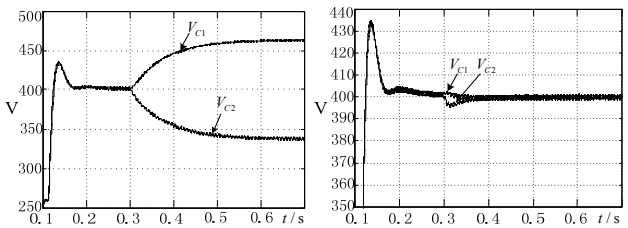

(a) (b)

Fig. 10. Simulation results of V_{C1} and V_{C2} (a) before, (b) after adding NPV control strategy when the loads are unbalanced.

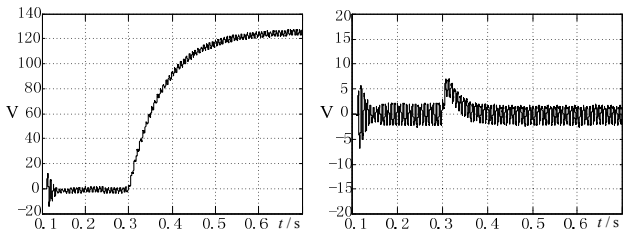

(a) (b)

Fig. 11. Simulation results of the NPV ΔV_C (a) before, (b) after adding NPV control strategy when the loads are unbalanced.

B. *Experiment Verification*

The hardware structure of the simulated direct-driven PMSG-based WPGS is shown in Fig. 12. In particular, it should be pointed out that, since the purpose of this paper is to verify the application performance of the Vienna rectifier in the generator-side of direct-driven PMSG-based WPGSs, the grid-connected side is not considered for the time being, and it is marked by a grey box in Fig. 12. The experiment is performed with a 10 kW simulated direct-driven PMSG-based wind power generation setup, as shown in Fig. 13. Fig. 13(a) and 13(b) show the PMSG driving system and the hardware layout of the Vienna rectifier, respectively. As can be seen in Fig. 13(a), the PMSG is driven by a three-phase asynchronous motor, and the asynchronous motor is driven by a 11 kW ABB frequency converter Type-ACS800-01-0016-3+P901.

The specifications of the PMSG are given in Table III. In addition, the filter capacitors C_1 and C_2 are both 470 uF, i.e., C_1=C_2=470uF. Moreover, the generator-side of the direct-driven PMSG-based WPGS is controlled by a TI digital signal processor (DSP) Type-TMS320F28335 and the switching frequency is 20 kHz.

Fig. 14(a) and 14(b) show the output orthogonal square pulse signals A and B of the PEE under the conditions of the PMSG natural rotation and reversal, respectively. From Fig. 14(a) and 14(b) it can be seen that there is a 90° phase difference between pulse-A and pulse-B. Furthermore, when the PMSG rotates naturally, pulse-A has a 90° phase delay to pulse-B. However, when the PMSG is reversed, pulse-B has a 90° phase delay to pulse-A. Therefore, the rotation direction of the PMSG rotor can be obtained by the relative positions of pulse-A and pulse-B.

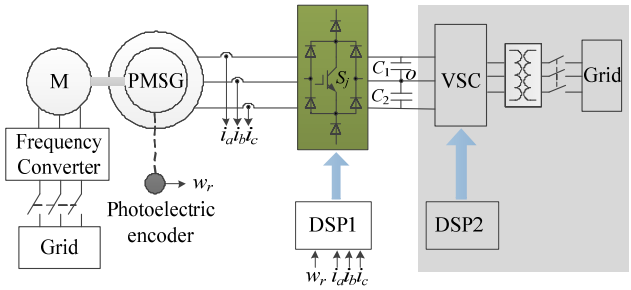

Fig. 12. Hardware diagram structure of the simulated direct-driven PMSG-based grid-connected WPGS in the laboratory.

(a)

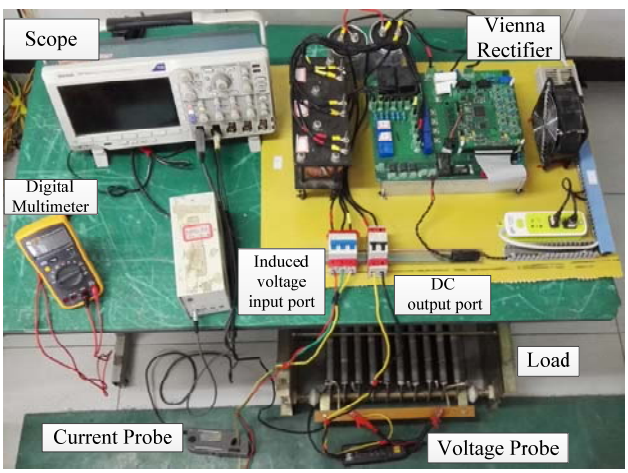

(b)

Fig. 13. Pictures show of the experiment verification setup (a) PMSG driving system. (b) Hardware layout of the Vienna rectifier.

TABLE III
SPECIFICATION OF PMSG

Specifications	Abbreviation	Value
Rated power	P_R	10 kW
Rated voltage	V_R	380 V
Rated speed	r_R	400 rpm
Pull-in torque	T	4 N·M
Pole-pairs	p_0	8
Efficiency	η	90%
Self-inductor	L_s	28 mH
Resistance of windings	R_s	1.2 Ω
Maximum PM flux	Ψ_{rmax}	1.462 Wb

kW = kilowatt, V = voltage, rpm = revolutions per minute, mH = milli herry, Wb = weber.

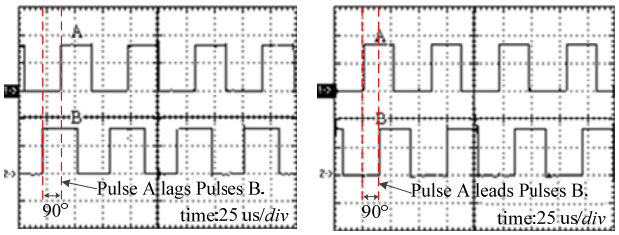

(a) (b)

Fig. 14. Square pulse signals of PEE under the conditions of (a) PMSG natural rotation. (b) PMSG reversal.

Fig. 15 shows waveforms of the induced voltage e_a and the estimated phase angle θ_e under the conditions of different rotating speeds of the PMSG rotor. From the experiment results of Fig. 15 (a) and (b) it can be seen that when the rotating speed of the PMSG changes, the phase angle and induced voltage can be accurately obtained. Therefore, the need for unit power factor operation can be guaranteed .

Fig. 16 (a) and (b) are the experiment results when the DC load R_L is added to and cutoff from the system, respectively. The system power and DC bus reference voltage are 1725 W, 3 kW and 250 V, 500 V in Fig. 18 (a) and (b), respectively. The waveforms in Fig. 20 shows that the stator current can start or stop smoothly when the load is suddenly changed.

Fig. 17 gives the waveforms when the system runs in the state of unit power factor under the conditions of different rotating speeds. The system power is 600 W and 1.8 kW in Fig. 17 (a) and (b), respectively. The DC bus reference voltage is 120 V and 300 V in Fig. 17 (a) and (b), respectively. The experiment results of Fig. 17 (a) and (b) illustrated that the phase of stator current can accurately track the phase of the induced voltage and that the power factor is approximately equal to 1. Therefore, it is apparent that the reactive loss of the PMSG can be significantly reduced.

In addition, the THD of the a-phase current, as shown in Fig. 17(b), is measured by a power quality analyzer-type FLUKE 43B, as shown in Fig. 18. It can be seen that the current frequency is 13.3Hz and the total harmonic distortion (THD) is 3.1% which is at a comparatively low level.

At last, the NPV control strategy is verified by experimental results, as shown in Fig. 19. In addition, the system power and the DC bus reference voltage are kept the same as Fig. 17(b). Fig. 19 (a) shows the experiment results without the NPV control strategy when the loads are unbalanced. Obviously, the voltages of C_1 and C_2 are unequal when the loads are unbalanced, as shown in Fig. 19(a). Meanwhile, when the NPV control strategy is added to the control system, the voltages of C_1 and C_2 are kept balanced, as shown in Fig. 19 (b). It can be seen from Fig. 19 that the experiment results are consistent with the simulation results in Fig. 10. Therefore, it can be concluded that both the experimental and simulation results verify the effectiveness of the adopted NPV control strategy.

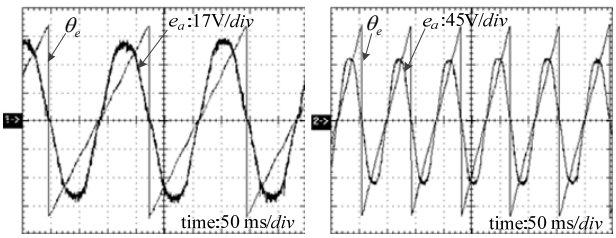

(a) (b)

Fig. 15. Experiment results of phase and induced voltage sensing in different rotate speeds of PMSG. (a) Rotate speed is 40 rpm. (b) Rotate speed is 80 rpm.

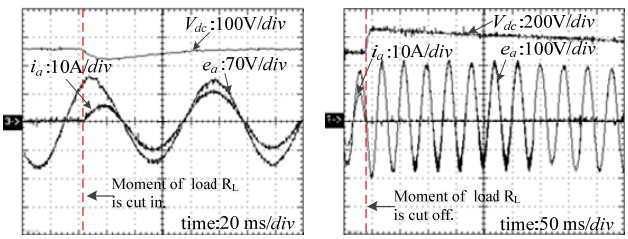

(a) (b)

Fig. 16. Experiment results when load changes suddenly. (a) Load R_L is added to the system suddenly from the state of non-load, rotate speed is 94 rpm. (b) load R_L is cutoff from the system suddenly, rotate speed is 166 rpm.

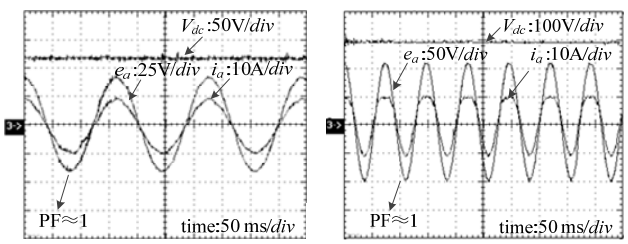

(a) (b)

Fig. 17. Experiment results of unit power factor in different speed. (a) Rotate speed is 37 rpm. (b) Rotate speed is 90 rpm.

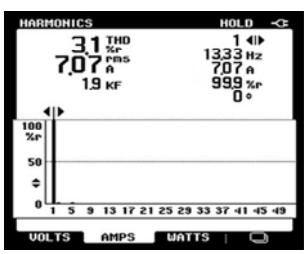

Fig. 18. Harmonic contents of a-phase current

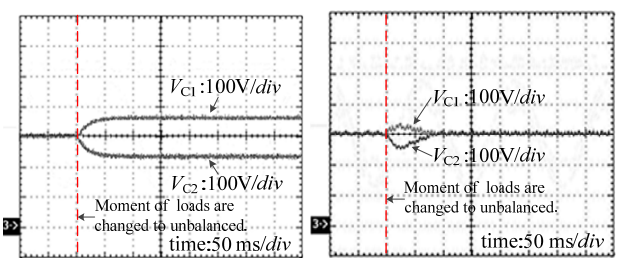

(a) (b)

Fig. 19. Experiment results of V_{C1} and V_{C2} (a) before, (b) after adding NPV control strategy when the loads are unbalanced.

VI. CONCLUSION

This paper uses the Vienna rectifier as the generator-side converter of a direct-driven PMSG-based WPGS to rectify the AC output voltage of a PMSG in the laboratory. Through the proposed method, the position of the rotor (the position of pulse-Z) is detected by using pulse-A, pulse-B and pulse-Z of the PEE, and the induced voltage is accurately obtained. As a consequence, the stator current maintains its synchronization with the induced voltage, and the DC bus voltage can track the reference value. Moreover, the reactive loss of the PMSG can be reduced. Meanwhile, the utilization rate of the PMSG's power capability can be increased. A simulation is performed to verify the performance of the Vienna rectifier when it is used in the generator-side of a direct-driven PMSG-based WPGS. In addition, a simulated direct-driven PMSG-based WPGS experiment setup was implemented to validate the proposed pulse-Z position detection method and the system performance. They confirm both the theory and the simulation results.

REFERENCES

[1] S. H. Lee, Y. Joo, J. Back, J. H. Seo, and I. Choy, "Sliding mode controller for torque and pitch control of PMSG wind power systems," *Journal of Power Electronics*, Vol. 11, No. 3, pp. 342-349, May 2010.

[2] J. Adhikari and S. Panda, "Overview of high altitude wind energy harvesting system," in *Power Electronics Systems and Applications(PESA)*, *2013 5th International Conference on*, pp. 1-8, 2013.

[3] J. Adhikari, A. Rathore, and S. Kumar Panda, "Modular interleaved softswitching dc-dc converter for high-altitude wind energy application," *IEEE J. Emeg. Sel. Topics Power Electron.*, Vol. 2, No. 4, pp. 727‑738, Dec 2014.

[4] I. Woofenden, How a Wind Turbine Works [Online]. Available: https:// homepower. com/articles /how-windturbine-works. 2016

[5] P. Pillay and R. Krishnan, "Modeling of permanent magnet motor drives", *IEEE Trans. Ind. Electron*., Vol. 35, No. 4, pp. 537-541, Nov. 1988.

[6] B. K. Bose, "Power electronics and AC machine drives-advances and trends," *International Power Electronics Congress, IEEE*, 2006.

[7] B. Wang, G. Wei, J. Chu, and G. Yi, " A novel modeling for a dual three-phase permanent magnet synchronous machines," *Control, Automation, Robotics and Vision, 2008. ICARCV 2008. 10th International Conference on IEEE*, pp. 1630-1634, 2008.

[8] Xu Ke, Hu Minqian, Yan Rong Yan, W Du, "Wind turbine simulator using PMSM", *Universities Power Engineering Conference, 2007*, pp. 732-737, 2007.

[9] M. A. Rahman, A. M. Osheiba, T. S. Radwan, and E. S. Abdin, "Modelingand controller design of an isolated diesel engine permanent magnet synchronous generator," *IEEE Trans. Energy Convers*., Vol. 11, No. 2, pp. 324-330, Jun. 1996.

[10] H. Geng, D. Xu, B. Wu, and G. Yang, "Active damping for PMSG based WECS with dc-link current estimation," *IEEE Trans. Ind. Electron*., Vol. 58, No. 4, pp. 1110-1119, Apr. 2011.

[11] A. Rajaei, M. Mohamadian, and A. Y. Varjani, "Vienna-rectifier-based direct torque control of PMSG for wind energy application," *IEEE Trans. Ind. Electron*., Vol. 60, No. 7, pp. 2919-2929, Jul. 2013.

[12] T. H. Nguyen and D. C. Lee, "Ride-through technique for pmsg wind turbines using energy storage systems," *Journal of Power Electronics*, Vol. 10, No. 6, pp. 733-738, Aug. 2010.

[13] T. Ahmed, K. Nishida, and M. Nakaoka, "Wind power grid integration of an IPMSG using a diode rectifier and a simple MPPT control for grid-side inverters," *Journal of Power Electronics*, Vol. 10, No. 5, pp. 548-554, Sep. 2010.

[14] H. Polinder, F. F. A. van der Pijl, G. J. de Vilder, and P. J. Tavner, "Comparison of direct-drive and geared generator concepts for wind turbines," *IEEE Trans. Energy Convers*., Vol. 21, No. 3, pp. 725-733, Sep. 2006.

[15] S. H. Song, S. Kang, and N. K. Hahm, "Implementation and control of grid connected AC–DC–AC power converter for variable speed wind energy conversion system," in *Proc. Appl. Power Electron. Conf. Expo.*, Vol. 1, pp. 154-158, 2003.

[16] S. M. Dehghan, M. Mohamadian, and A. Yazdian, "A new variable speed wind energy conversion system using permanent magnet synchronous generator and z-source inverter," *IEEE Trans. Energy Convers*., Vol. 24, No. 3, pp. 724-714, Sep. 2009.

[17] J. Wang, D. Xu, B. Wu, and Z. Luo, "A low-cost rectifier topology for variable-speed high-power PMSG wind turbines," *IEEE Trans. Power Electron*., Vol. 26, No. 8, pp. 2192-2200, Jan. 2011.

[18] J. Kikuchi, M. D. Manjrekar, and T. A. Lipo, "Complementary half controlled three phase PWM boost rectifier for multi-DC-link applications," in *Proc. 15th Annu. IEEE APEC,* pp. 494-500, 2000.

[19] Y. Wang, D. Panda, T. A. Lipo, and D. Pan, "Performance improvement of dual-half-controlled-converter and its applications in utility rectifiers," in *Proc. 8th Int. Conf. Power Electron./ECCE Asia, Jeju, Korea*, pp. 1711-1718, 2011.

[20] S. Zhang, K. Tseng, D. M. Vilathgamuwa, T. D. Nguyen, and X. Wang, "Design of a robust grid interface system for PMSG-based wind turbine generators," *IEEE Trans. Ind. Electron*., Vol. 58, No. 1, pp. 316-328, Jan. 2011.

[21] C. Hao and D. Aliprantis, "Analysis of squirrel-cage induction generator with Vienna rectifier for wind energy conversion system," *IEEE Trans. Energy Convers*., Vol. 26, No. 3, pp. 967-975, Sep. 2011.

[22] A. H. Rajaei, M. Mohamadian, S. M. Dehghan, and A. Yazdian, "PMSG-based variable speed wind energy conversion system using Vienna rectifier," *Eur. Trans. Elect. Power*, Vol. 21, No. 1, pp. 954-972, Jan. 2011.

[23] F. Blaabjerg, M. Liserre, and K. Ma, "Power electronics converters for wind turbine systems," *IEEE Trans. Ind. Electron*., Appl., Vol. 48, No. 2, pp. 708-719, Mar. 2012.

[24] M. Malinowski, S. Stynski, W. Kolomyjski, and M. P. Kazmierkowski, "Control of three-level PWM converter applied to variable-speed-type turbines," *IEEE Trans. Ind. Electron*., Vol. 56, No. 1, pp. 69-77, Jan. 2009.

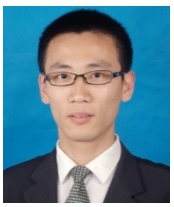

Hongyan Zhao was born in Hebei province, China, in 1988. He received his B.S. and M.S. degrees in Electrical Engineering from Yanshan University, Qinhuangdao, China, in 2010 and 2013, respectively. Since 2013, he has been working towards his Ph.D. degree in Electrical Engineering from Beijing Jiaotong University, Beijing, China. His current research interests include three-phase grid-connected systems, renewable power systems, and electric vehicles.

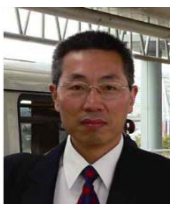

Trillion Q. Zheng (Qionglin Zheng) (M'06-SM'07) was born in Jiangshan, Zhejiang province, China, in 1964. He received his B.S. degree in Electrical Engineering from Southwest Jiaotong University, Sichuan, China, in 1986; and his M.S. and Ph.D. degrees in Electrical Engineering from Beijing Jiaotong University, Beijing, China, in 1992 and 2002, respectively. He is presently working as a University Distinguished Professor at Beijing Jiaotong University. He directs the Center for Electric Traction, founded by Ministry of Education, China. His current research interests include the power supplies and AC drives of railway traction systems, high performance and low loss power electronics systems, PV based converters and control, active power filters, and power quality correction. He holds 17 Chinese patents, and has published over 60 journal articles and more than 100 technical papers in conference proceedings. From 2003 to 2011, he served as the Dean in the School of Electrical Engineering, Beijing Jiaotong University. He is presently working as the Deputy Director of the Council of the Beijing Society for Power Electronics, and as a Member of the Council of the China Electrotechnical Society. He received an Excellent Teacher Award from the Beijing Government (1997), Youth Award of Railway Science and Technology of Zhan Tianyou (2005). He was Laureates of the Youth Elite of Science and Technology of the Railway Ministry of China (1998) and a Zhongda Scholar for the power electronics and motor drive area, by the Delta Environmental and Educational Foundation (2007).

Yan Li was born in Heilongjiang province, China, in 1977. She received her B.S. and M.S. degrees in Electrical Engineering from Yanshan University, Qinhuangdao, China, in 1999 and 2003, respectively; and her Ph.D. degree in Electrical Engineering from the Nanjing University of Aeronautics and Astronautics, Nanjing, China, in 2009. From 1999 to 2009, she was at Yanshan University, Hebei, China. Since 2009, she has been in the School of Electrical Engineering, Beijing Jiaotong University, Beijing, China. Her current research interests include multiple-input dc/dc converters, renewable power systems, and PV grid-tied systems.

Jifei Du was born in Tianjin, China, in 1986. He received his B.S. degree from School of Electrical Engineering, Tianjin University of Technology, Tianjin, China, in 2008. He is presently working towards his Ph.D. degree in Electrical Engineering from Beijing Jiaotong University, Beijing, China. His current research interests include power electronics, AC/DC and DC/DC converters, and electric vehicles.

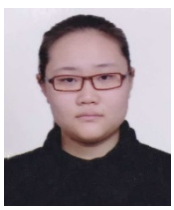

Pu Shi was born in Hebei province, China, in 1993. She received her B.S. degree in Electrical Engineering from Beijing University, Beijing, China, in 2015, where she is presently working towards her M.S. degree in Power Electronics. Her current research interests include high-frequency power conversion techniques and wide bandgap power semiconductor devices.